Composites Part C: Open Access 4 (2021) 100107

Contents lists available at ScienceDirect

Composites Part C: Open Access

journal homepage: www.elsevier.com/locate/jcomc

Performance of BFRP RC beams using high strength concrete

Farid Abed*, Mustafa Al-Mimar, Sara Ahmed

Department of Civil Engineering, American University of Sharjah, University City, PO Box 26666, Sharjah, UAE

ARTICLE INFO

Keywords:
BFRP
Flexure
Crack width
Bond-dependent coefficient
Deflection
High strength concrete

ABSTRACT

This research investigates the flexural behavior and serviceability performance of basalt fiber-reinforced polymer (BFRP) reinforced concrete (RC) beams cast with normal- and high-strength concretes (NSC and HSC). Carbon FRP (CFRP) and steel-reinforced concrete beams were also included for comparison purposes. Four-point bending tests were performed on a total of 14 slender beams with dimensions of 180 mm × 230 mm × 2200 mm. The main aim was to examine the improvement in the performance of BFRP RC beams using HSC and to assess its compatibility with the recommendations and guidelines of the ACI440 Code. The test results were reported and discussed in terms of flexural capacity, deflection, crack width, reinforcement and concrete strains, and failure modes. The results revealed that the flexural capacities of BFRP beams were slightly underestimated by ACI440.1R-15 while reasonable predictions were observed for the cracking moments in HSC and NSC. The use of HSC as compared to NSC enhanced the cracking and ultimate moments of all BFRP RC beams by 10% and 16%, respectively. Furthermore, the average bond-coefficient (k_b) value for BFRP-RC beams was found to be 0.70 which is much lower than the conservative k_b value suggested by the ACI440 guidelines for sand-coated FRP bars.

1. Introduction

The vulnerability of conventional steel bars in concrete structures to corrosion makes fiber-reinforced polymer (FRP) bars a more attractive alternative. FRP bars in concrete have been used since the 1980s, mostly in harsh environments. Their commonly used types include carbon fiber-reinforced polymer (CFRP), aramid fiber-reinforced polymer (AFRP), and glass fiber-reinforced polymer (GFRP). In addition to their non-corrosive characteristic, FRPs are environmentally friendly, non-toxic, magnetic insulators with high strength to weight ratio, and of low densities. These characteristics makes FRPs easy to handle and cost effective [1–4]. Despite the aforementioned advantages, FRPs in general exhibit linear-elastic behavior until failure, and possess no ductility as compared to conventional steel bars. Since these materials have a low elastic modulus as compared to steel, they exhibit larger deflections and wider crack widths; thus they are designed in terms of serviceability limit states [5–8]. The ACI 440–1R-15 [9] recommends that FRP-RC members should be designed to be over-reinforced, i.e., fail by concrete crushing, to provide a degree of deformability before failure.

In recent years, a newly developed type of FRP, known as basalt fiber-reinforced polymer (BFRP), has emerged and gained wide attention over the past few years due to its economic advantage over GFRP and CFRP composites. Although current design codes ACI 440.1R-15 [9] and CSA S806–12 [10] provide recommendations on FRPs as main reinforcement, there are still no material specifications and design codes for BFRPs specifically. Therefore, research is still required to investigate the factors that affect the performance of BFRP-RC elements. The research herein focuses on evaluating the flexural behavior of RC beams reinforced with BFRP bars using normal and high strength concrete (NSC and HSC).

Several studies showed that BFRP bars have acceptable mechanical and durability characteristics. For example, El Refai et al. [11] and Altalmas et al. [12] studied the effect of different environmental exposures on the bond stress-slip response, adhesion to concrete, and bond strength of BFRP bars. The results showed that the bond characteristics were mainly governed by surface treatment and manufacturing quality rather than the fiber type. All specimens failed by inter-laminar shear between the FRP layers rather than shear stress between the bar and concrete. A number of recent studies were also conducted to evaluate the effect of BFRP reinforcing bars on the flexural and shear behavior of concrete beams [13–17]. Tomlinson and Fam [13] tested nine slender concrete beams with BFRP flexural reinforcement ratios ranging from 0.28 to 1.60. The experimental results were well predicted by ACI 440.1R-06 and CSA S806–12 equations, and indicated that the ultimate and service loads were directly related to the flexural reinforcement ratio regardless of the failure mode. El Refai and Abed [14] investigated the shear behavior of ten BFRP-reinforced concrete beams with no transverse reinforcement. The results confirmed that the shear behav-

* Corresponding author.
E-mail addresses: fabed@aus.edu (F. Abed), b00036309@alumni.aus.edu (M. Al-Mimar), g00049654@alumni.aus.edu (S. Ahmed).

https://doi.org/10.1016/j.jcomc.2021.100107
Received 27 December 2020; Accepted 8 January 2021

Fig. 1. Photos of types and sizes of bars used in this study.

Table 1
Mechanical properties of the rebars.

Sample designation	Cross sectional area A (mm^2)	Ultimate tensile stress f_u (MPa)	Ultimate strain ε_u (%)	Modulus of elasticity E (GPa)
BFRP 8	57.4	1075.1 ± 37	2.1 ± 0.1	42.9 ± 1.4
BFRP 10	58.4	1028.7 ± 47	2.4 ± 0.1	42.8 ± 1.3
BFRP12	121.3	1118.6 ± 31	2.4	46.6 ± 1.7
BFRP16	211.9	1121.3 ± 56	2.4	46±2.1
CFRP12	113	2068	1.58	131
Steel 10	78.5	460 (yield)	0.23 (yield)	200
Steel 12	113	460 (yield)	0.23 (yield)	200

ior of the tested BFRP-reinforced beams was similar to GFRP-reinforced beams. Ovitigala et al. [15] studied the serviceability and ultimate load behavior of beams reinforced with different BFRP bar sizes of 10, 13, 16, and 25 mm. It was shown that increasing the reinforcement ratio up to a certain limit had greater influence on reducing the beam deflection than increasing the moment capacity. Also, the ultimate moment capacity was found to be underestimated by the ACI code while the ultimate and post cracking strains were in good agreement with the code's predicted results. A study conducted by Elgabbas et al. [16] showed that the increase in reinforcement ratio causes a non-linear increase in the moment capacity of BFRP RC beams. The average bond-dependent coefficient was estimated to be 0.76 for the sand-coated BFRP bars and the cracking moment was overestimated by both ACI 440.1R-15 [9] and CSA S806–12 [10].

The aim of this study is to investigate the flexural response and serviceability of BFRP RC beams using high and normal strength concrete. The use of HSC is expected to be very effective in enhancing the flexure performance and cracking behavior of FRP-reinforced beams [18]. It not only enhances the concrete response at the compression side but also makes efficient use of the tensile strength of the FRP bars. The test parameters of the present experimental program mainly include the BFRP reinforcement ratio, reinforcement type (BFRP versus CFRP and steel) and concrete strength (HSC vs. NSC). The effect of each of these parameters on the flexural capacity, deflection and cracking behavior as well as reinforcement and concrete strains is studied. The experimental results of the cracking and ultimate moments as well as the bond-dependent coefficient (k_b) are employed to assess the design equations of the ACI 440.1R code [9].

2. Experimental program

2.1. Materials

2.1.1. Rebars

Two types of sand-coated FRP rebars were used in this study: BFRP bars of 8, 10, 12- and 16-mm diameter, and CFRP bars of 12-mm diameter. Steel bars of diameters 10- and 12-mm were also used. Fig. 1 shows the types and sizes of bars used in the study. The BFRP bars were supplied from Galen, a manufacturing company located in Russia. The CFRP bars were manufactured and supplied by Structural Technologies LLC in the United States. Samples from these bars were tested to obtain their mechanical properties, namely, the ultimate tensile strength, tensile stain, and elastic modulus. Table 1 presents the mechanical properties of all bars.

2.1.2. Concrete

Two types of concrete mixes, which will be referred to as normal strength concrete (NSC) and high strength concrete (HSC), were developed in this study. The concrete mix designs per cubic meter are shown in Table 2. The target concrete compressive strengths were 35 MPa for NSC and 65 MPa for HSC. However, on the testing day, the cube compressive strengths for the normal- and high- strength mixes were found to be 47.5 and 70.5 MPa, respectively.

2.2. Specimen configuration and test matrix

Beams were designed to have a cross section of 180 mm × 230 mm to satisfy the ACI 440.1R-15 code recommendations in terms of clear cover, bar spacing, minimum required depth (one tenth of the clear span), and span-to-depth ratio ($a/d \geq 3$) to ensure the specimens are slender. Fig. 2 shows the reinforcement and cross-sectional details of the beam specimens. The clear span of the beams was set to be 1900 mm with an additional 150 mm extension on each side, adding to a total length of 2200 mm, to provide adequate development length for FRP bars. Steel stirrups of 10 mm diameter were provided in the shear span at 100 mm spacing. All FRP-RC beams were designed to be over-reinforced, i.e., have a reinforcement ratio that is greater than the balanced reinforcement ratio to fail in flexure by concrete crushing.

A total of fourteen beams were prepared and tested in flexure. Seven of these beams were cast using the HSC mix while the other seven were cast using the NSC mix. The main aim was to study the flexural performance of BFRP-reinforced beams using normal and high strength concrete. The variables considered in the present test matrix included the reinforcement ratio, reinforcement type, and concrete compressive strength. The designation of the beams was selected to represent the size and number of bars, bar type and concrete compressive strength. The first number denotes the number of main reinforcement bars in each beam. The letter T and the number next to it indicates the diameter of reinforcing bars in millimeters. The letters B, C and S denote the types of reinforcing bars which are BFRP, CFRP and steel, respectively. The last letter symbolizes the concrete compressive strength of the beam. For instance, beam 3T8B-N is reinforced with 3 BFRP bars that are 8 mm in diameter and cast with normal concrete compressive strength (NSC). The details of the 14 beams are shown in Table 3.

2.3. Test setup and instrumentation

A four-point loading test setup, shown in Fig. 3, was utilized in this study to evaluate the flexural response of all beams. All tests were conducted using the universal testing machine (UTM) with 2000 KN loading

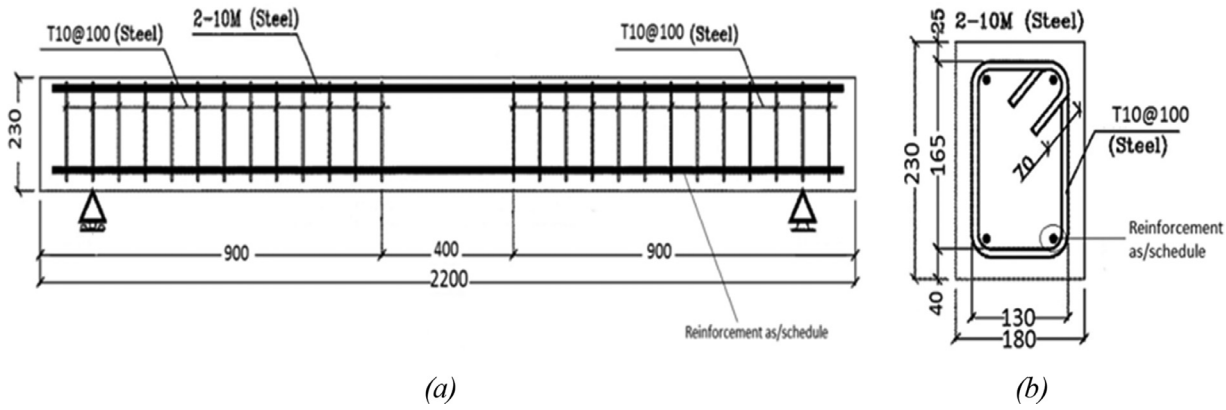

Fig. 2. Beam specimen; (a) reinforcement details and (b) cross-section.

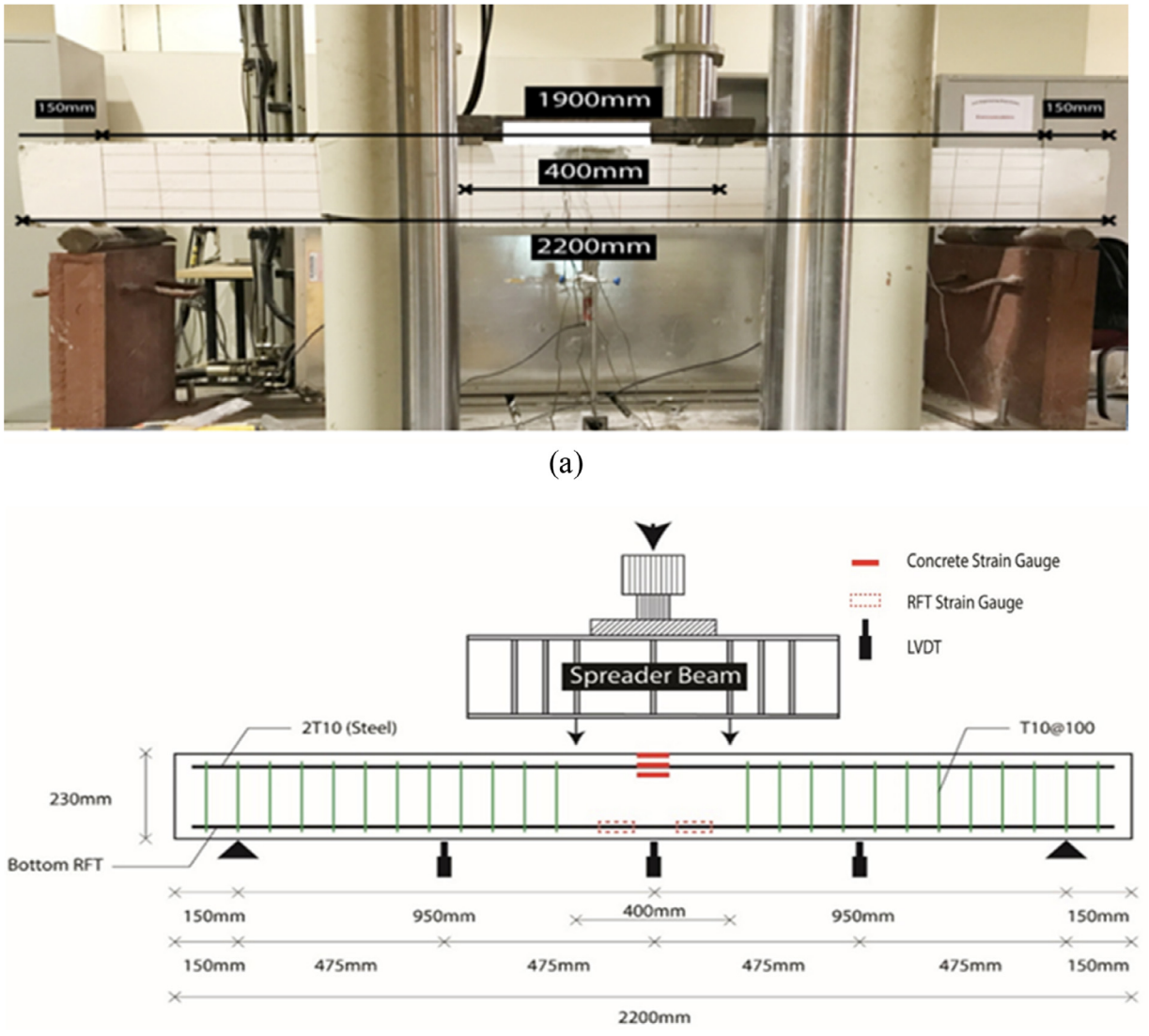

Fig. 3. Beam test setup;(a) beam under UTM machine, (b) illustration of setup and instrumentation.

Table 2
Concrete mix designs.

Concrete Mix	Unit Weight (Kg/m3) Cement	Water	3/4" Cr Aggregate	3/8" Cr Aggregate	3/8 Cr Sand	Dune Sand	Additives	Total Unit Weight
NSC	350	168	518	420	640	314	5	2415
HSC	430	153	459	420	643	284	47.5	2436.5

Table 3
Test matrix details.

Beam	Bar Type	Bar Size (mm)	A (mm^2)	EA (MN)	ρ_f	ρ_f/ρ_{fb}
3T8B-N	BFRP	8	3T8=172	7.5	0.00448	1.90
2T10B-N	BFRP	10	2T10=171	7.85	0.00471	1.85
2T12B-N	BFRP	12	2T12=243	11.3	0.00682	2.90
3T16B-N	BFRP	16	3T16=636	30.15	0.0184	7.97
2T12C-N	CFRP	12	2T12=243	29.6	0.00682	3.73
2T10S-N	Steel	10	2T10=157	31.4	0.00471	0.16
2T12S-N	Steel	12	2T12=226	45.2	0.00682	0.23
3T8B-H	BFRP	8	3T8=172	7.5	0.00448	1.45
2T10B-H	BFRP	10	2T10=171	7.85	0.00471	1.4
2T12B-H	BFRP	12	2T12=243	11.3	0.00682	2.2
3T16B-H	BFRP	16	3T16=636	30.15	0.0184	6.03
2T12C-H	CFRP	12	2T12=243	29.6	0.00682	2.84
2T10S-H	Steel	10	2T10=157	31.4	0.00471	0.12
2T12S-H	Steel	12	2T12=226	45.2	0.00682	0.18

Table 4
Experimental and predicted ultimate and cracking moments.

Beam	Experimental M_n (KN.m)	δ (mm)	M_{cr} (kN.m)	Exp./Pred. ACI [9] M_n	M_{cr}	Failure Mode
3T8B-N	23.00	36	6.49	1.11	1.07	CC
2T10B-N	22.80	40	6.56	1.09	1.08	CC
2T12B-N	31.10	34	6.10	1.23	1.01	CC
3T16B-N	38.30	30	6.00	1.05	0.99	CC
2T12C-N	41.60	35	6.08	1.11	1.00	CC
2T10S-N	21.00	23	6.83	1.30	1.13	TC
2T12S-N	24.40	14	6.38	1.08	1.05	TC
3T8B-H	26.00	36.2	7.65	1.10	1.04	CC
2T10B-H	24.80	38	7.36	1.03	1.00	CC
2T12B-H	31.90	44	6.90	1.11	0.93	CC
3T16B-H	44.50	31	6.75	1.05	0.91	CC
2T12C-H	50.30	34	8.06	1.14	1.09	CC
2T10S-H	22.29	29.2	7.10	1.34	0.96	TC
2T12S-H	26.60	24.5	6.77	1.15	0.92	TC
Average	–	–	–	1.14	1.01	–
Standard deviation	–	–	–	0.09	0.06	–

CC: Concrete Crushing; TC: Tension Control (steel yielding).

capacity (Fig. 3a). The load was applied using hydraulic jacks directly on the spreader beam which transfers the load equally into two loading points on the beam over a constant moment span of 400 mm. Strain gauges were mounted on the reinforcing bars prior to casting and on the concrete beams prior to testing to record the strains throughout each test. LVDT's were fixed at the beam soffit to measure the vertical deflection. Crack transducers were also utilized to measure crack widths during the tests.

3. Results and discussions

3.1. Cracking moment

The load at first crack was monitored visually during the test for all beams and recorded for comparison with the code predictions. All beams showed similar behavior until first cracking. The reinforcement ratio had negligible effect on the first cracking load. Table 4 summarizes the experimental and predicted cracking and ultimate moments for all NSC and HSC beams along with their mid-span deflections and failure modes.

The average cracking moment for all NSC beams was 6.34 kN.m (ranged from 6.0 to 6.83 kN.m), which is close to the cracking moment values predicted by the ACI code equation [9]. On the other hand, the cracking moments for HSC beams ranged from 6.9 to 8.06 kN.m with an average of 7.1 kN.m. Increasing the compressive strength from 47.5 to 70.5 MPa led to an increase in the cracking moment by approximately 10%. The predicted values for the cracking moments were found to be quite similar to the experimental cracking moments for most of the HSC beams. Different findings were reported by Elgabbas et al. [19] where the cracking moment was 27% lower than those predicted by ACI [9] for BFRP-RC beams. The lower cracking moments reported in [19] were attributed to the additional stresses from shrinkage, temperature effect, and freezing and thawing of water inside the concrete, which may have resulted in lower cracking loads than predicted. In this study, however, the cracking moment results seem to be compatible with ACI 440.1R-15, as shown in Table 4. The average experimental to predicted cracking moment for all beams was found to be 1.01±0.06. In general, the cracking moment values were mostly in the range of 21 to 30% of the ultimate moment capacity.

Table 5
Experimental bond dependent coefficient (k_b).

Beam ID	$0.30M_n$	$w = 0.7$mm	Average
3T8B-N	0.48	0.43	0.46
2T10B-N	0.46	0.78	0.62
2T12B-N	0.42	0.49	0.46
3T16B-N	1.27	1.06	1.16
2T12C-N	0.80	1.05	0.93
3T8B-H	0.52	0.40	0.46
2T10B-H	0.62	0.38	0.50
2T12B-H	0.50	0.63	0.56
3T16B-H	0.62	0.78	0.70
2T12C-H	1.08	1.32	1.20
Average	0.68	0.73	0.70
Standard Deviation	–	–	0.28

3.2. Bond-dependent coefficient (k_b)

Since FRP bars have a low modulus of elasticity compared to steel, the design of flexural members is often controlled by serviceability requirements. The design for the crack width can either follow a direct or indirect procedure: direct by determining the crack width explicitly, and indirect by specifying the maximum bar spacing limits. Both methods require the determination of the bond coefficient, k_b, to account for the bond between the FRP bars and surrounding concrete, which affects the crack width. An extensive analysis was conducted by the ACI committee on a variety of concrete cross-sections and FRP bar manufacturers, resin formulations, fiber types, and surface treatments to evaluate the k_b values. The ACI [9] committee suggests that a value of 1.4 should be used when the k_b factor is unknown from experimental data, whereas, the CAN/CSA S6 [10] recommends using a value of 0.8 for sand-coated bars.

The service load level still does not have a fixed definition in design codes. Several studies assume that the service load occurs at approximately 30% of the nominal flexural capacity. In this study, the k_b values were obtained both at $0.30M_n$ and at a crack width of 0.70 mm as shown in Table 5. The average k_b value for all sand-coated BFRP and CFRP bars was found to be 0.70. The k_b factor results demonstrate that the 1.4 value suggested by the ACI code may be too conservative on average for the sand-coated BFRP bars. The 0.70 average value, however, seem to be closer to the 0.80 factor suggested by CAN/CSA S6 for the sand-coated bars. Similar findings were reported in [19].

3.3. Crack width and propagation

All beams were found to exhibit traditional flexural cracking behavior. Flexural cracks appeared in the constant moment region once the concrete's tensile strength was exceeded. The flexural cracks propagated slowly from the constant moment region to the compression face of the concrete where crushing occurred. The flexural cracks were affected by a combination of flexural and shear stresses while propagating out of the pure bending zone and thus tended to gain a horizontal component. Fig. 4 illustrates the cracking behavior at the service and ultimate stages for all beams. As observed, increasing the reinforcement ratios led to a different crack behavior and distribution for both NSC and HSC beams. In other words, increasing BFRP reinforcement increased the number of cracks which therefore reduced the crack spacing (beams 2T10B vs. 2T12B and 3T16B) for both NSC and HSC.

Since FRPs are resistant to corrosion, the guidelines and codes permit larger crack width for FRP-RC elements than for steel reinforced concrete members. Considerations for FRP crack width control include aesthetics, creep rupture, and shear effects. As per CAN/CSA S806 and CAN/CSA S65 codes, crack widths for up to 0.5- and 0.7-mm are allowed for exterior and interior exposure, respectively. The ACI 440.1R recommends using CAN/CSA S806 in most of the cases. In addition, since the crack width is directly affected by the strain in the FRP reinforcing bars, the ISIS Manual No. 3 specifies a strain limit of 0.002 to control the crack width. Fig. 5 shows the moment versus crack width for NSC and HSC beams with different reinforcement types. The crack width increased gradually with the increase in moment; however, the increasing trends were slightly different. Increasing the reinforcement ratio provided stiffer moment vs. crack width trend as was the case for the 2T12B and 3T16B beams when compared with the 2T10B beam for both concrete compressive strengths.

The effect of the number of reinforcing bars on the propagation of the cracks widths was also noticeable. For example, for the same reinforcement ratio, BFRP-RC beams reinforced with 3 bars (3T8B) showed stiffer moment versus crack width relationships than the BFRP beam reinforced with only two bars (2T10B), as illustrated in Fig. 5(a) and 5(b). This behavior was more apparent for HSC beams than NSC beams. Similar results were reported in [16] and [19] regarding the increase of number of bars in concrete beams. This agrees with the ACI440.1R-15 equation, since reducing spacing between bars should reduce the crack width of the beams.

For beams with different types of reinforcing bars but with almost the same axial stiffness (3T16B, 2T12C & 2T10S), the BFRP- and CFRP-RC beams (3T16B & 2T12C) showed some similarities in their cracking behavior at service loading for both concrete strengths, as shown in Fig. 5(c) and 5(d). On the other hand, beams reinforced with conventional steel bars (2T10S) started to deviate prior to yielding with larger crack widths at smaller moments. When comparing the cracking width response between the two different types of FRP bars for the same reinforcement ratio (2T12C vs. 2T12B), beams reinforced with CFRP bars (2T12C) exhibited smaller crack width values at high moments compared to the beams reinforced with BFRP bars (2T12B) due to the high stiffness CFRP bars exhibit. This response is clearly illustrated in Fig. 5(c) and 5(d) for NSC and HSC, respectively.

3.4. Flexural capacity and mode of failure

All FRP-RC beams were designed to fail by concrete crushing when the concrete reaches its ultimate strain of 0.003. This is the common design approach for FRP beams according to ACI 440.1R-15 [9] and CAN/CSA S806–12 [10]. The ultimate capacity of the beams along with the failure mode is presented in Table 4 and Fig. 6. As designed, all FRP-RC beams were observed to fail by concrete crushing whereas the conventional steel-RC beams failed by steel yielding, i.e., tension-controlled failure. The beams with the highest BFRP reinforcement ratio (3T16B) had the highest flexural capacity, followed by beams 2T12B, 2T10B and 3T8B, respectively (see Table 4). Note that beams 3T8B and 2T10B have similar stiffnesses (7.5 and 7.85 MN) and reinforcement ratios (0.00448 and 0.00471), which resulted in similar ultimate capacities of 23 and 22.8 MPa for the NSC mix, and 26 and 24.8 MPa for the HSC mix.

The effect of increasing the BFRP reinforcement ratio on the improvement in the load-bearing capacity of BFRP RC beams is shown in Fig. 7. For NSC beams, increasing the reinforcement ratio by 44.7 and 290% (2T12B and 3T16B with respect to 2T10B) increased the moment capacity by 36 and 68% (31.1 and 38.3 MPa with respect to 22.8 MPa), respectively. A slightly different trend was observed for HSC beams where the corresponding moment capacities increased by 28.6 and 79.4% (31.9 and 44.5 MPa with respect to 24.8 MPa), respectively. The nonproportional increasing trend of the flexural capacity agrees well with the ACI 440.1R-15 [9] moment equation for compression-controlled failure mode, as illustrated in Fig. 7.

It can also be noticed that the percentage improvement in the moment capacities of BFRP RC beams due to a nearly 50% increase in concrete compressive strength was 8.7% for the lower BFRP reinforcement ratio (2T10B), but increased up to 16.2% at the higher BFRP reinforcement ratio (3T16B). This is attributed to the fact that delaying the concrete failure at the compressive zone allows the FRP bars to strain more and consequently attain higher resistance/strength, thus positively contributing to the overall flexural capacity of the beam based on their axial

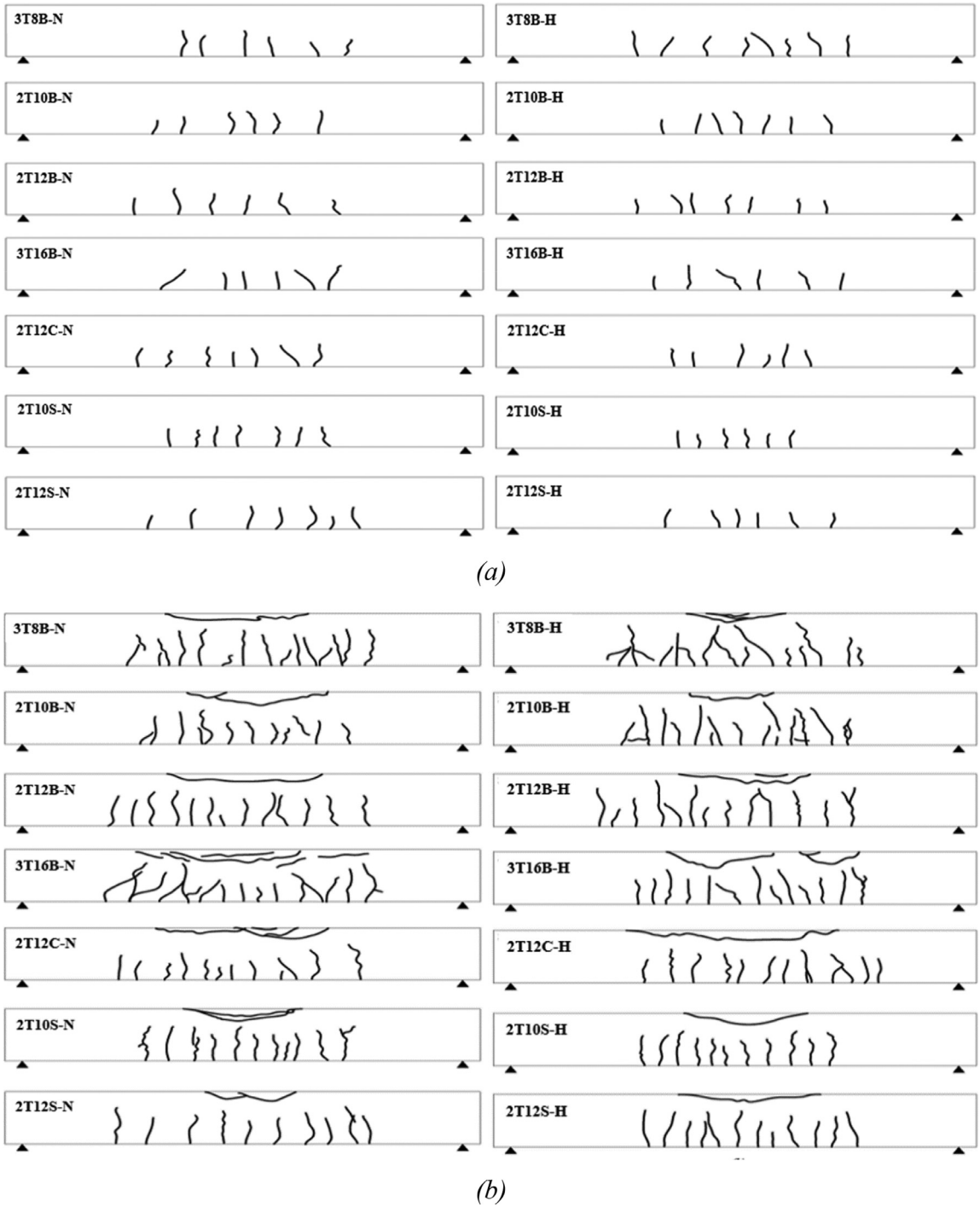

Fig. 4. Crack pattern at (a) service load stage, (b) ultimate load stage.

stiffnesses. For the case of CFRP RC beams (2T12C), an improvement of up to 21% in the flexural capacity was recorded due to the 50% increase in f'_c.

A comparison of the flexural capacity of BFRP beams with other types of reinforcement (CFRP and steel) was also evaluated. For the same axial stiffness (EA ~ 30 MN) but different reinforcement ratios (3T16B vs. 2T12C and 2T10S), the CFRP RC beam showed a comparable flexural capacity to the BFRP RC beam with a variation of less than 8% for the case of NSC beams but up to 12% for the case of HSC beams, as listed in Table 4. However, both types of FRP reinforcements recorded much higher moment capacities than steel-reinforced beams with an increase up to 98% and 130% for NSC and HSC, respectively. On the other hand, for FRP and steel beams of similar reinforcement ratios (2T12B, 2T12C, and 2T12S), CFRP RC beams showed much higher moment capacity than BFRP RC beams, which is evidently attributed to the higher elastic modulus (i.e., axial stiffness) of CFRP as compared to BFRP bars, as listed in Table 1. Furthermore, the flexural capacity of the 2T12B and 2T12C beams were higher than that of the 2T12S by 27 and 71% for NSC and 20 and 89% for HSC, respectively.

The ratios of the experimental to predicted flexural capacity of all beams can be shown in Table 4. The predicted moment capacity was calculated as per the moment equations specified by AC1 440 for FRP-

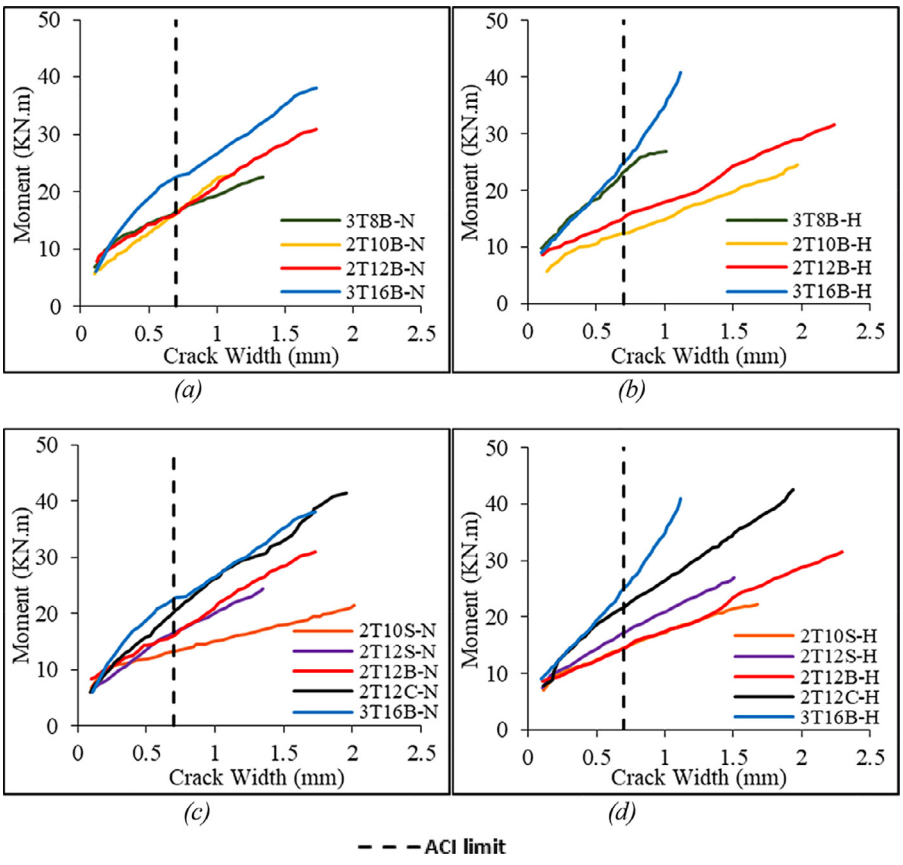

Fig. 5. Moment vs. Crack Width (a) different BFRP reinforcement ratios with NSC, (b) different BFRP reinforcement ratios with HSC, (c) different reinforcement types with NSC, and (d) different reinforcement types with HSC.

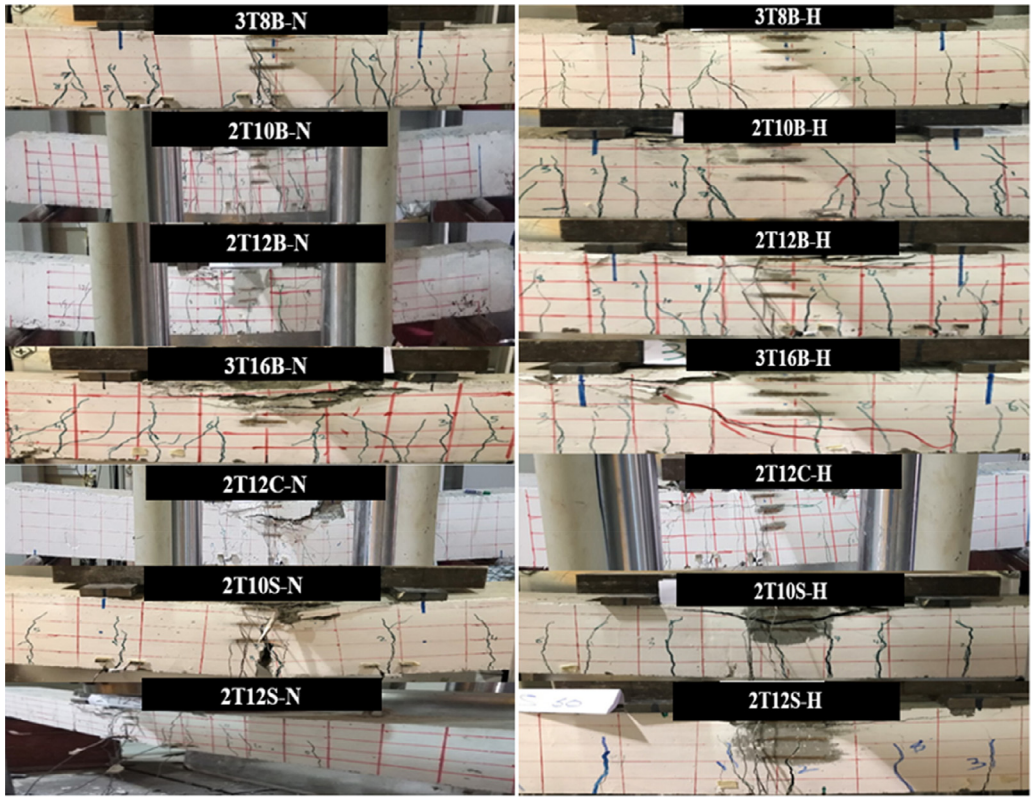

Fig. 6. Failure modes of all beams: (a) NSC and (b) HSC.

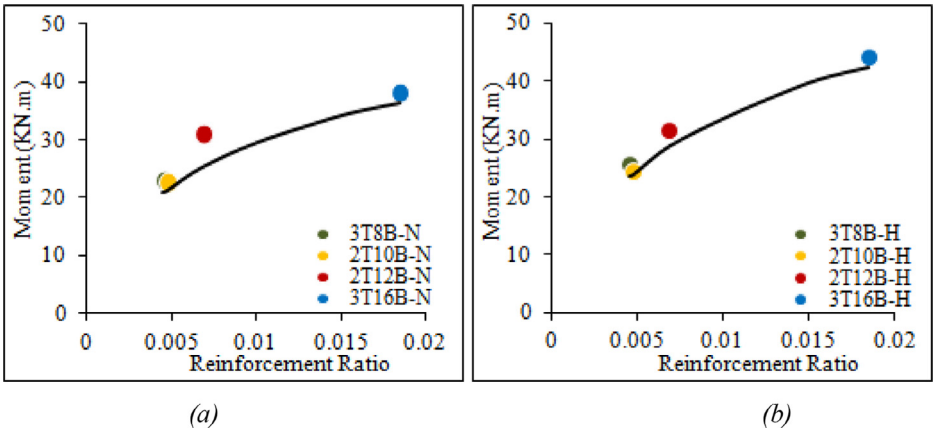

Fig. 7. ultimate moment vs. reinforcement ratio curve: (a) NSC and (b) HSC.

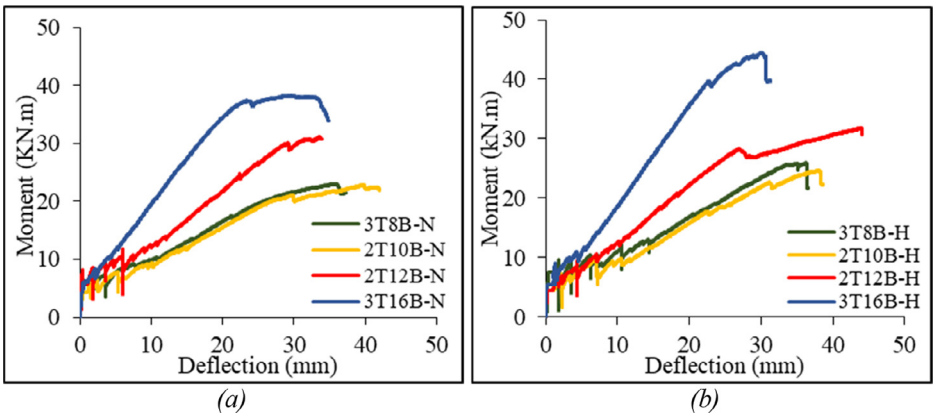

Fig. 8. Moment vs mid-span deflection for different reinforcement ratios: (a) NSC and (b) HSC.

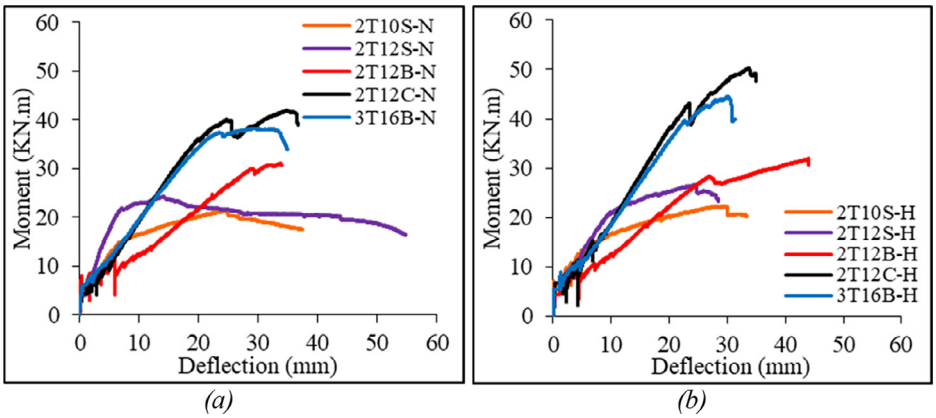

Fig. 9. Moment vs mid-span deflection for different reinforcement types: (a) NSC and (b) HSC.

RC beams and ACI-318 for steel-RC beams. In general, the ultimate capacities of the beams were slightly underestimated by the ACI code. Similar observations were reported in [15]. The average experimental to predicted ultimate capacity of the beams was found to be 1.14±0.09.

3.5. Deflection behavior

The moment versus mid-span deflection response of all beams can be shown in Figs. 8 and 9. The effect of using different BFRP reinforcement ratios on the moment versus mid-span deflection curves is illustrated in Fig. 8a and 8b for the NSC and HSC beams, respectively. At early stages and prior to cracking, the BFRP reinforcement ratio had negligible effect on the first cracking moment (see Table 4) as all beams showed similar deflection behavior, indicating similar stiffnesses at this stage. After cracking, however, the reinforcement ratio had a significant effect on the deflection behavior, as seen in the decrease in the slopes due to the reduced stiffness. From Fig. 8a and b, BFRP RC beams of the same axial stiffness (2T10B and 3T8B) experienced almost the same flexural response for both concrete mixes. However, the beams reinforced with 3 bars showed slightly lower deflection than that of the beams reinforced with 2 bars (3T8B vs. 2T10B) for both NSC and HSC. Similar results were reported by Abed and Alhafiz [20] on the effect of the number of bars on mid-span deflection. Increasing the reinforcement ratio led to a higher post-cracking stiffness in the beams, which therefore resulted in better deflection behavior and lower deflection values (for more details see Fig. 8 and Table 4). Beams with the highest BFRP reinforcement ratio and stiffness (3T16B) experienced the lowest deflection at the ultimate moment compared to other BFRP RC beams. The deflection values for the 3T16B beam were 30 and 31 mm for the NSC and HSC, respectively.

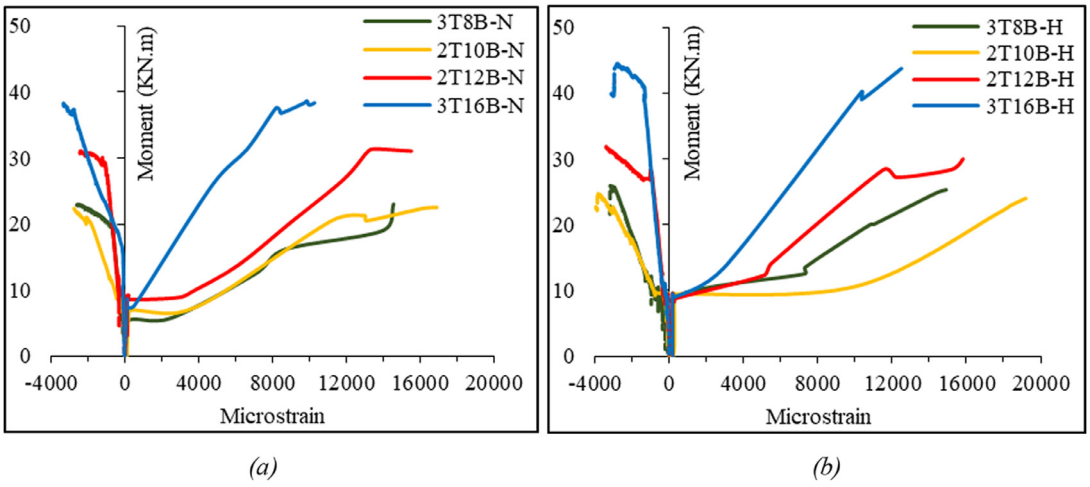

Fig. 10. Recorded strains in longitudinal reinforcement and concrete for different reinforcement ratios: (a) NSC and (b) HSC.

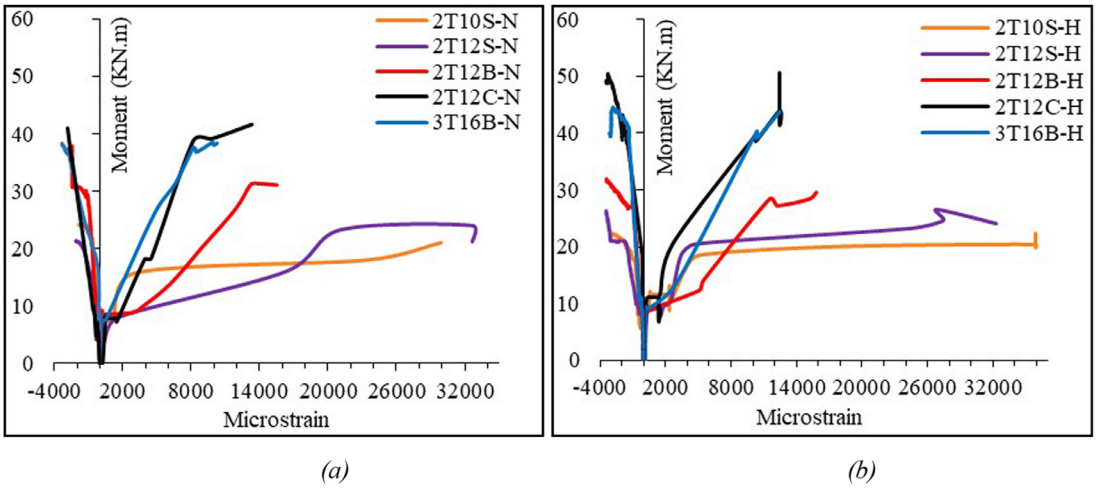

Fig. 11. Recorded strains in longitudinal reinforcement and concrete for different reinforcement types: (a) NSC and (b) HSC.

Fig. 9, on the other hand, shows the deflection behavior for the NSC and HSC beams reinforced with different reinforcement types (BFRP, CFRP & steel). The FRP beams of the same axial stiffnesses (3T16B & 2T12C) did not show significant differences in their deflection behavior. The 2T12C beam showed slightly better load-deflection performance than the 3T16B beam for both types of concrete mixes. As for the steel reinforced beam with the same EA (2T10S), the load-deflection behavior was fairly close to the FRP beams up to the steel yielding point.

For the case of concrete beams having the same reinforcement ratios (2T12B, 2T12C & 2T12S), 2T12C beam showed lower deflection values, followed by 2T12B beams and 2T12S beams, for the same load level. In addition, increasing the concrete strength of the beams led to a slight enhancement in the flexural capacity and deflection for all beams.

3.6. Reinforcement and concrete strain

Figs. 10 and 11 show the strain values of longitudinal reinforcement at the tension side and of concrete at the compression side, captured using strain gauges installed at the mid-span of the reinforcement and concrete sections. All beams showed similar pre-cracking response, followed by a significant post-cracking increase in FRP tensile strains until failure. This is due to the reduced post-cracking stiffness associated with the FRP bars. The concrete and reinforcement strains at ultimate loads for all beams are summarized in Table 6. As the reinforcement ratio increases, the reinforcement strain decreases. The beams with the highest ρ (3T16B) showed the lowest reinforcement strains of 0.0105 and 0.013 for beams cast with NSC and HSC, respectively. Similar results were reported in [16,20,21]. The two BFRP beams with similar EA (3T8B & 2T10B) showed some similarities in strain values, as shown in Fig. 10. However, the ultimate strain of the beams reinforced with two bars (2T10B) was higher than that of the beam reinforced with 3 bars (3T8B) for both normal- and high-strength concrete.

In general, BFRP-reinforced beams cast with HSC mixes exhibited higher compression strains at the top fibers as compared to their NSC counterparts. This, in turn, helped engage the BFRP bars, thus enhancing the flexural capacity of the HSC beams. However, the percentage improvement in the moment capacity is still not proportional to the percentage increase in concrete compressive strength.

Fig. 11 shows comparisons of the strain responses for beams with different types of longitudinal reinforcement (BFRP vs. CFRP & steel). For the beams with the same ρ (2T12B, 2T12C & 2T12S), steel showed the highest reinforcement strain compared to basalt and carbon at the maximum loads. Increasing the compressive strength from 47.5 MPa to 70.5 MPa for beams of the same type slightly decreased the strain after cracking at the same load level. A linear relationship between moment and strain was noticed in the FRP bars for NSC and HSC beams, with a steeper slope for CFRP bars due to their high(er) elastic modulus. At higher moments, CFRP bars exhibited lower strain values compared to BFRP bars. A similar comparison of the strain response was made between concrete beams of the same EA (3T16B, 2T12C, & 2T10S) where

Table 6
Reinforcement and concrete strains at ultimate moments.

Beam	Moment (kN.m)	Concrete Strain	Longitudinal Reinforcement Strain
3T8B-N	23.00	0.0026	0.014
2T10B-N	22.80	0.0028	0.016
2T12B-N	31.10	0.0025	0.015
3T16B-N	38.30	0.0033	0.0105
2T12C-N	41.60	0.0028	0.013
2T10S-N	21.00	0.0021	0.029
2T12S-N	24.40	0.0019	0.032
3T8B-H	26.00	0.0032	0.016
2T10B-H	24.80	0.0038	0.019
2T12B-H	31.90	0.0034	0.015
3T16B-H	44.50	0.0028	0.013
2T12C-H	50.30	0.0034	0.012
2T10S-H	22.29	0.0030	0.035
2T12S-H	26.60	0.0034	0.027

both FRP bars showed comparable strain responses but with strain values much lower than that of steel bars, as shown in Fig. 11. At the ultimate moments, the reinforcement strains of 2T12C, 2T12B, and 2T12S beams were 0.013, 0.015, and 0.032 for NSC, and 0.012, 0.015, and 0.028 for HSC, as listed in Table 6.

4. Summary and conclusion

This research investigated the flexural behavior and serviceability performance of BFRP-RC beams using two concrete mixes of 47 MPa (NSC) and 70 MPa (HSC) cube compressive strengths and compared them to CFRP-and steel-RC beams. The experimental program involved testing a total of 14 beams: seven beams cast with NSC and seven others cast with HSC. The flexural tests were conducted using a four-point loading test. The beams were 180 mm × 230 mm × 2200 mm in dimension and had a clear span of 1900 mm. All FRP bars were sand coated, with bar sizes of 8, 10, 12, and 16 mm for BFRP, and 12 mm for CFRP. The sizes of the steel bars were 10 and 12 mm. The following conclusions can be drawn within the scope of this investigation:

- The use of HSC mixes enhanced the cracking moment of all BFRP RC beams by around 10% when compared to NSC beams. The ACI equation was found to be satisfactory in predicting the modulus of rupture for NSC and HSC beams. The BFRP reinforcement ratio had negligible effect on the cracking moment.
- The average bond-dependent coefficient k_b for BFRP-RC beams was found to be around 0.70 which indicates a good bond between the sand-coated FRP bars and surrounding concrete. The results suggest that the value of 1.4 recommended by the ACI 440 may be very conservative.
- The flexural capacity was significantly affected by the BFRP reinforcement ratio (ρ) and reinforcement type. The increasing trend of the flexural capacity for BFRP-RC beams with increasing ρ agrees well with the ACI 440.1R-15 moment equation for the compression-controlled failure mode. The average experimental to predicted moment capacity for all beams was reported as 1.14±0.09. Furthermore, HSC beams showed up to 16% increase in the ultimate moments as compared to NSC beams.
- The reinforcement ratio had a negligible effect on the deflection and strain values of all beams at initial stages prior to cracking. A typical bilinear curve for deflection and strain was observed for the BFRP-RC beams until failure. However, after cracking, beams with the highest reinforcement ratio showed the lowest deflection and strain values due to the increased stiffness. Also, for beams of the same stiffness, increasing the number of bars led to lower values of deflection and strain.
- The deflection behavior was affected by the type of reinforcement. For beams with the same axial stiffness (EA), the deflection behavior of both BFRP- and CFRP-RC beams were almost similar as compared to steel-reinforced beams. For beams with the same ρ, the CFRP beam (highest EA) showed better deflection behavior followed by BFRP then steel.
- Increasing the reinforcement ratio and stiffness increased the amount of absorbed energy which enhanced the cracking behavior for the BFRP-RC beams. The 3T8B and 3T16B beams showed better cracking performance than 2T10B and 2T12B beams, mainly for having 3 bars. In general, FRP-RC beams showed smaller crack width with high moment values as compared to steel-RC beams. Beams with same stiffness are expected to have similar behavior.
- The reinforcement strain decreased with the increase in reinforcement ratio for the BFRP-RC beams. However, the CFRP-RC beam showed slightly different load vs. strain relationship as compared to BFRP-RC beam with the same EA.

Data availability statement

The raw/processed data required to reproduce these findings cannot be shared at this time as the data also forms part of an ongoing study.

Declaration of Competing Interest

The authors declare that they have no known competing financial interests or personal relationships that could have appeared to influence the work reported in this paper.

Acknowledgement

The authors would like to acknowledge the financial support provided by the American University of Sharjah (grant No. IRF-002).

References

[1] N. ElMessalami, F. Abed, A. El Refai, Fiber-reinforced polymers bars for compression reinforcement: a promising alternative to steel bars, Constr. Build. Mater. 209 (2019) 725–737.
[2] M.N. Habeeb, A.F. Ashour, Flexural behavior of continuous GFRP reinforced concrete beams, J. Compos. Constr. 12 (2) (2008) 115–124, doi:10.1061/(ASCE)1090-0268(2008)12:2(115).
[3] F. Abed, H. El-Chabib, M. Alhamaydeh, Shear characteristics of GFRP-reinforced concrete deep beams without web reinforcement, J. Reinf. Plast. Compos. 31 (16) (2012) 1063–1073, doi:10.1177/0731684412450350.
[4] M.M. Rafi, A. Nadjai, F. Ali, Experimental testing of concrete beams reinforced with carbon FRP bars, J. Compos. Mater. 41 (22) (2007) 2657–2673, doi:10.1177/0021998307078727.
[5] J. Cai, J. Pan, X. Zhou, Flexural behavior of basalt FRP reinforced ECC and concrete beams, Constr. Build. Mater. 142 (2017) 423–430, doi:10.1016/j.conbuildmat.2017.03.087.
[6] A. Al-Tamimi, F. Abed, A. Al-Rahmani, Effects of harsh environmental exposures on the bond capacity between concrete and GFRP reinforcing bars, Adv. Concrete Constr. 2 (2014) 1 v..
[7] P. Escórcio, P.M. França, Experimental study of a rehabilitation solution that uses GFRP bars to replace the steel bars of reinforced concrete beams, Eng. Struct. 128 (2016) 166–183, doi:10.1016/j.engstruct.2016.09.013.

[8] A.El Refai, F. Abed, A. Al-Rahmani, Structural performance and serviceability of concrete beams reinforced with hybrid (GFRP and steel) bars, Constr. Build. Mater. J. 96 (2015) 518–529 v..
[9] ACI 440.1R-15Guide for the Design and Construction of Structural Concrete Reinforced with Fibre-Reinforced Polymer (FRP) bars. ACI committee 440, American Concrete Institute, Farmington Hills, 2015.
[10] CAN/CSA S806-12Design and Construction of Building structures with Fibre-Reinforced Polymer, Canadian Standards Association, Ontario,Canada, 2012.
[11] A.El Refai, F. Abed, A. Altalmas, Bond durability of basalt fiber-reinforced polymer bars embedded in concrete under direct pullout conditions, J. Compos. Constr. 19 (5) (2015) 1–11, doi:10.1061/(ASCE)CC.1943-5614.0000544.
[12] A. Altalmas, A. El Refai, F. Abed, Bond degradation of basalt fiber-reinforced polymer (BFRP) bars exposed to accelerated aging conditions, Constr. Build. Mater. (2015), doi:10.1016/j.conbuildmat.2015.02.036.
[13] D. Tomlinson, A. Fam, Performance of concrete beams reinforced with basalt FRP for flexure and shear, J. Compos. Constr. 19 (2) (2015) 1–10, doi:10.1061/(ASCE)CC.1943-5614.0000491.
[14] A. El Refai, F. Abed, Concrete contribution to shear strength of beams reinforced with basalt fiber-reinforced bars, J. Compos. Constr. 20 (4) (2016), doi:10.1061/(ASCE)CC.1943-5614.0000648.
[15] T. Ovitigala, M.A. Ibrahim, M.A. Issa, Serviceability and ultimate load behavior of concrete beams reinforced with basalt fiber-reinforced polymer bars, ACI Struct. J. 113 (4) (2016) 757–768, doi:10.14359/51688752.
[16] F. Elgabbas, E.A. Ahmed, B. Benmokrane, Flexural behavior of concrete beams reinforced with ribbed basalt-FRP bars under static loads, J. Compos. Constr. 21 (3) (2017), doi:10.1061/(ASCE)CC.1943-5614.0000752.
[17] F. Abed, A. El Refai, S. Abdalla, Experimental and finite element investigation of the shear performance of BFRP-RC short beams, Structures 20 (2019) 687–701 v..
[18] A. El-Nemr, E.A. Ahmed, B. Benmokrane, Flexural behavior and serviceability of normal- and high-strength concrete beams reinforced with glass fiber-reinforced polymer bars, ACI Struct. J. 110 (6) (2013) 1077–1087.
[19] F. Elgabbas, P. Vincent, E.A. Ahmed, B. Benmokrane, Experimental testing of basalt-fiber-reinforced polymer bars in concrete beams, Compos. Part B Eng. 91 (2016) 205–218, doi:10.1016/j.compositesb.2016.01.045.
[20] F. Abed, A.R. Alhafiz, Effect of basalt fibers on the flexural behavior of concrete beams reinforced with BFRP bars, Compos. Struct. 215 (February) (2019) 23–34, doi:10.1016/j.compstruct.2019.02.050.
[21] A. El-Nemr, E.A. Ahmed, C. Barris, B. Benmokrane, Bond-dependent coefficient of glass- and carbon-FRP bars in normal- and high-strength concretes, Constr. Build. Mater. 113 (2016) 77–89, doi:10.1016/j.conbuildmat.2016.03.005.